



47th SME North American Manufacturing Research Conference, Penn State Behrend Erie,
Pennsylvania, 2019

Feasibility of Metal Additive Manufacturing for Fabricating Custom Surgical Instrumentation for Hip and Knee Implants

Sudhanshu Nahata^a, O. Burak Ozdoganlar^{a,b,c,*}

^aDepartment of Mechanical Engineering, Carnegie Mellon University, Pittsburgh, PA 15213, USA

^bDepartment of Material Science and Engineering, Carnegie Mellon University, Pittsburgh, PA 15213, USA

^cDepartment of Biomedical Engineering, Carnegie Mellon University, Pittsburgh, PA 15213, USA

Abstract

The prevailing approaches for fabrication of orthopedic surgery instruments involve specialized machining processes on cast or stock parts. For high-volume fabrication of those instruments, machining is the most cost-effective approach. However, many trial components and various patient-specific (and/or physician-specific) tools and instruments have complex geometries and are needed only in very small batches sizes. Towards addressing this strong need for efficient manufacturing of customized surgical instruments for hip and knee implant surgeries, in this work, we performed a feasibility study by using a selective laser melting (SLM) process for this purpose. Additively manufactured (AM) 316L stainless steel parts (in both as-built and stress relieved conditions) were compared with the traditionally manufactured components from nominally the same material for both mechanical properties and microstructure. To improve the surface roughness of the AM parts, three different surface finishing post-processes were evaluated to achieve the required roughnesses better than 1.5 microns R_a . Experiments are then conducted to evaluate the effect of AM process parameters, including the laser power, hatch spacing and raster speed, on the resulting as-built surface quality. Lastly, two sample surgical instruments were fabricated and post-processed to demonstrate the methodology. Overall, the use of metal AM for fabrication of custom surgical instrumentation is deemed feasible and promising.

© 2019 The Authors. Published by Elsevier B.V.

This is an open access article under the CC BY-NC-ND license (<http://creativecommons.org/licenses/by-nc-nd/3.0/>)

Peer-review under responsibility of the Scientific Committee of NAMRI/SME.

Keywords: additive manufacturing; surgical instruments; stainless steel 316L; surface finishing; material characterization; hip and knee surgery; laser melting

1. Introduction

There is a strong demand for customized surgical instrumentation for hip and knee arthroplasty surgeries [1]. These surgical instruments are of complex and curved designs with extensive diversity of geometries, and are fabricated at very small production volumes, possibly as low as a few devices per design per year. Currently, each implant is accompanied by a large set of standard and customized instruments. In addition, there is an increasing demand by orthopedic surgeons for modified and/or customized instrumentation [2, 3, 4, 5]. The economical impact of these complex instrumentation is very significant, reaching up to 70% of the manufacturing costs in medical prosthesis industry. Due to the unique combined characteristics of very low production volumes, complex designs, and short

fabrication times, effective and economical manufacturing of customized surgical instrumentation for hip and knee implants poses considerable challenges for traditional manufacturing approaches. Although customization of instruments brings exciting opportunities for innovating new designs that can have significant impact in the success of surgical outcomes, the lack of cost- and time-effective manufacturing approaches can hinder potential advances [6, 7].

One of the manufacturing approaches that could address this challenge is metal additive manufacturing (AM). Many advances during the last decade now enables AM to be used as an effective means of fabricating functional products in a variety of markets [8], including aerospace [9, 10] and medical devices [11, 12]. The current technology covers a relatively large number of materials, with newer alloys constantly under development. A large portion of the research in AM is devoted to medical device applications, such as scaffolds and implants [13, 14, 15, 16].

There has been a considerable amount of research in the manufacturing literature on achieving fully dense parts using

* Corresponding author. Tel.: +1-412-268-9890; e-mail: ozdoganlar@cmu.edu.

two powder-bed based AM processes: electron beam melting (EBM) and selective laser melting (SLM) [17]. Research is also underway for evaluation and optimization of AM processes to obtain reproducible and uniform material characteristics on the fabricated parts. Recent works presented assessment of material properties, such as tensile strength, elastic modulus, elongation and hardness, for a varying set of process parameters and build orientations [14, 18, 19, 20]. Another area of research is the assessment of part quality of additively manufactured parts, including dimensional accuracy [21], porosity [22, 23] and surface roughness [24, 25]. Research to date indicated that the final material properties depend strongly on the selection of powder, process environment, AM technology, process parameters, built orientation and built location [18]. As such, each material used with a given AM technology and system require a thorough qualification to identify the effect of process parameters on material and quality characteristics of fabricated parts.

In this work, we present a feasibility study for using a powder-bed based direct laser melting AM process and the associated system to fabricate customized surgical instruments from 316L austenitic stainless steel (SS). The material properties are required to satisfy the ASTM F899-12b “Standard Specification for wrought Stainless Steels for Surgical Instruments”, and dimensional tolerances within $\pm 125\ \mu\text{m}$ and micron-level surface roughness (e.g., better than $1.5\ \mu\text{m}$) are required [26, 27]. First, using a set of parameters provided by the machine manufacturer for 316L stainless steel material, a custom-designed artifact is fabricated to characterize the geometric accuracy and repeatability of the process. Measurement of specific features on the artifact are completed using an automated coordinate measurement machine (CMM). Second, a set of tensile test specimens were fabricated, again using the recommended parameter set but at different print orientations. Tensile tests were then performed on both those samples and traditionally-fabricated (rolled and machined) samples in order to compare material properties and evaluate whether they satisfy the ASTM F899-12b standard. Further material characterization and comparison were then completed, including indentation hardness and microstructural evaluations. Next, towards satisfying the surface roughness requirements for surgical instruments, various finishing processes are evaluated to improve the surface quality of AM-fabricated components. Additionally, a study is conducted to optimize the up-skin parameter set to improve the surface roughness of the as-built part. Finally, to demonstrate the AM process and the finishing approaches, two customized surgical instruments were fabricated.

2. Experimental Methods

2.1. Materials and Manufacturing

In this work, 316L stainless steel was used with a chemical composition complying to ASTM F899-12b [27]. The SLM machine (EOS M 290) used for printing the samples uses a Yb-fiber laser with a maximum power output of 400 W and a laser spot size of 70 microns [28]. Since powder plays an im-

portant role in imparting the resulting material properties, the 316L powder used in the experiments was acquired directly from the machine manufacturer. Unless otherwise noted, the following default “core” printing parameters (recommended by EOS) were used during the experiments: layer thickness of $20\ \mu\text{m}$, laser power of 195 W, and raster speed of 1,083 mm/s. The default laser scanning strategy was used, where the laser beam was rotated by 67 deg. between subsequent layers.

Post-print heat treatment is typically required for SLM parts due to the presence of residual stresses originating as a result of rapid cooling [29]. Therefore, some of the test samples were heat treated (stress relieved) in an electrical furnace within an inert atmosphere. For this purpose, the SAE standard AMS2759 [27] for heat treatment of austenitic corrosion-resistant steel parts was followed. According to the recipe, the parts were soaked at 899°C for a specific time, depending on the thickness of the part, followed by slow cooling. For instance, an 8 mm thick tensile test specimen was soaked for 45 minutes at 899°C and brought to room temperature by slow cooling that took 6 hours.

2.2. Assessment of Dimensional Accuracy, Surface Roughness and Repeatability

To evaluate the dimensional accuracy and repeatability of the as-built samples, an in-house developed quality-standard artifact (QSA) [30] (See Fig. 1(a)-(b)) was used. The QSA possesses a range of features that enable assessment of dimensional accuracy, repeatability, surface quality, as well as identification of minimum feature size that the system can print for a particular parameter set. For our case, we focused on regions A and B of the QSA. Region A consists of a 5×5 array of 3 mm square pillars separated by a distance of 6 mm, and Region B consists of a variable-height staircase. A coordinate measurement machine (CMM) with a measurement accuracy of 2 microns (Zeiss DuraMax) was used for quantitative assessment.

The surface roughness was measured using a focus-variation based microscope that is capable of providing the 3D surface profile (Alicona InfiniteFocus). The vertical and lateral resolution are selected to be 100 nm and $5\ \mu\text{m}$, respectively. To represent surface roughness, we used average areal surface roughness (S_a).

2.3. Mechanical and Microstructural Characterization

A uniaxial tensile testing machine was used to measure a range of mechanical properties, including yield strength (σ_y), ultimate tensile strength (σ_u), elastic modulus (E), and ductility (% elongation). An extension rate of 1.5 mm/min was used for the tests. The axial displacement in the elastic regime was measured using a strain gauge (KFH-6-350-C1-11L1M2R, Omega Inc.) A quarter-bridge configuration was used for strain gauge measurements. The tensile test specimens were manufactured according to the ASTM E8 “sub-size” specifications [31]. These samples were printed in three different orientations to assess the effect of print direction [32]. Fig. 2 displays the three print directions used for the experiments: horizontal

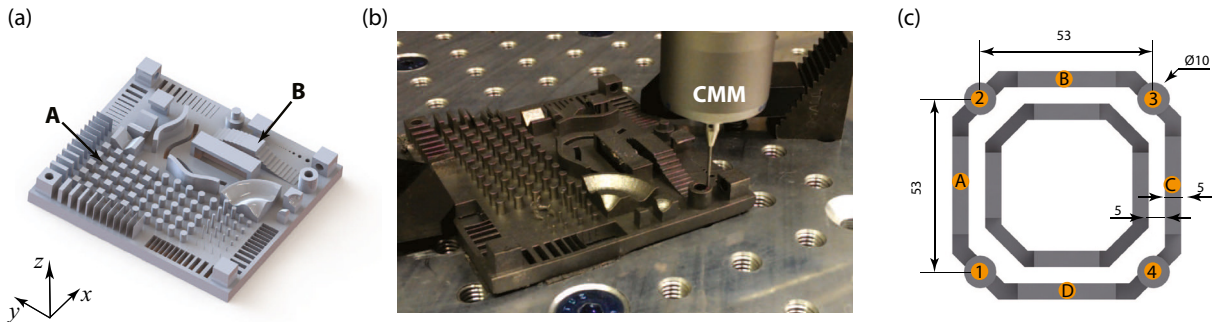


Fig. 1. (a)-(b) In-house developed quality standard artifact (QSA) to evaluate dimension and position accuracy, and (c) simple calibration part for scaling, provided by machine manufacturer.

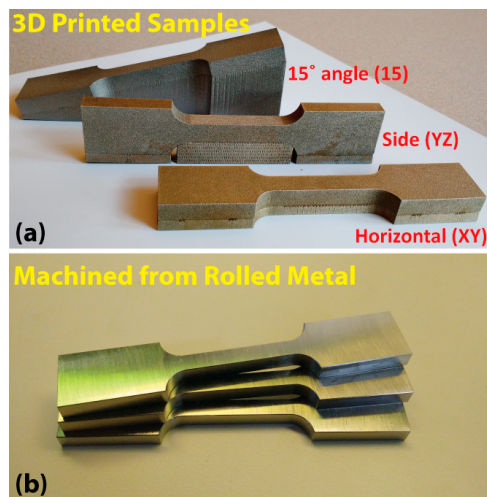


Fig. 2. Tensile test samples: (a) printed samples with SS 316L, and (b) samples made from traditionally-manufactured material.

(XY), side (YZ) and at 15° angle with the horizontal plane (15). These specimens were printed slightly larger in size and were machined afterwards to the exact size in order to remove any unwanted effects coming from surface-flaws/roughness and to ensure the sample dimensions are accurate.

The microstructure of the samples were studied using an optical microscope. The samples were polished and etched to reveal the microstructure with an intent to measure the grain size. The planar grain size was calculated using the line intercept method (ASTM E112-12 [33]). To measure the hardness, a Rockwell-B hardness tester was used. This tester uses a tungsten ball indenter with 1.5875 mm diameter. The specimen for hardness testing was prepared in accordance with ASTM E18-15 [34]. A five-point average is taken when reporting the results.

To qualify the AM-built parts for use as surgical instruments, the aforementioned properties of the AM-built specimens are compared with traditionally-fabricated (rolled and machined) 316L samples. The 316L used for traditionally-fabricated samples is solution annealed (min. 1900°F) and adheres to the UNS 31600/31603 standard.

3. Results and Discussion

3.1. Dimensional and Location Accuracy

Table 1 provides the measurement results from region A and B shown in Fig. 1(a). The mean widths in the x and y directions are found to be smaller than the nominal width, outside of the targeted ± 0.125 mm tolerance, with a small standard deviation. This deviation in the mean width may be attributed to the shrinkage of the material during cooling. A small standard deviation of $11 \mu\text{m}$ between the features suggests that the shrinkage is relatively uniform. The mean difference in z -height is $17 \mu\text{m}$, which falls well within the tolerance. The standard deviation for the z -height measurements is relatively higher than that for the $x - y$ measurements; this could be due to the limited resolution in z as a result of finite layer thickness of $20 \mu\text{m}$.

Although the above results indicate that the process lacks the required accuracy, the low standard deviation values attest to the precision of the process. As such, accurate part dimensions may be obtained by changing the prescribed dimension parameters during printing. For this purpose, to correct the shrinkage in the $x - y$ plane, dimensional scaling factors were iteratively obtained by using a relatively simpler calibration part (see Fig. 1(c)), provided by the machine manufacturer. This part consists of two sets of 5 mm thick walls located at 5 mm apart (at regions A, B, C and D), and four 10 mm diameter cylindrical posts (at regions 1, 2, 3 and 4). To quantify the shrinkage, we measured the wall thickness and the wall-to-wall distance. The scaling factors were increased if the measured thickness is smaller than the nominal and vice versa. This iterative procedure is concluded when the measurement results are within $\pm 125 \mu\text{m}$ (see Tab. 2). The obtained scaling factors were then used to print the rest of the samples in the manuscript.

Table 1. Measurement results from the QSA. The dimensions are in mm.

Features	Nominal	Measured	StDev
x-width (A)	3.000	2.800	0.009
y-width (A)	3.000	2.786	0.008
c-c x-distance (A)	6.000	5.995	0.011
c-c y-distance (A)	6.000	5.992	0.011
z-height difference (B)	0.000	0.017	0.034

Table 2. Measurement results from the simple calibration part.

	Outside	Inside	Nominal value
A [mm]	5.091	4.927	5.000
B [mm]	5.095	4.907	5.000
C [mm]	5.092	4.929	5.000
D [mm]	5.087	4.902	5.000

3.2. Mechanical and Material Testing

The mechanical and material testing is performed for samples with three different processing condition: traditionally manufactured (rolled and machined), as-built (no heat treatment), and stress relieved (heat treated).

3.2.1. Tensile tests

A stress-strain curve is obtained for each of the samples from the uniaxial tensile tests. The stress-strain plot for the as-built specimens and the traditionally-manufactured samples are plotted in Fig. 3. These curves were used to determine the mechanical properties given in Table 3. The 0.2%-offset method was used to calculate σ_y of the material.

As expected, heat treatment had a relatively large effect on the mechanical properties of the samples: The σ_y of heat treated (HT) samples were found to be up to 20% higher than the that of the as-built samples. After heat treatment, the σ_y for the additively manufactured 316L reached to within 22 MPa (10%) of the traditionally manufactured samples. The tensile strength for all the tested samples were found to be comparable with less than 5% deviation from the traditionally-manufactured samples. The elastic modulus for the as-built samples were found to be 10 GPa (~5%) lower than both the heat treated and the traditionally-manufactured samples. The largest difference between the traditionally manufactured and AM-built samples was observed in the amount of elongation before fracture. Where the rolled samples elongate over 72%, the AM-built samples only elongated between 40-50%. This decrease in the elongation (toughness) is possibly due to the process-induced defects, which may be improved using hot isostatic pressing (HIP) treatment [35].

Table 3. Tensile testing results. HT represent heat treated samples.

Sample	σ_y (MPa)	σ_u (MPa)	E (GPa)	Elongation (%)
Rolled	320	640	193	72.36
XY	251	662	178	43.78
HT-XY	318	659	188	43.63
YZ	280	645	179	43.76
HT-YZ	298	628	188	47.02
15	276	660	180	50.24
HT-15	322	647	189	49.42

3.2.2. Hardness Testing

The hardness of the samples were tested on both the top (the plane normal to the build direction) and the side (the plane parallel to the build direction) surfaces. For the rolled samples, the

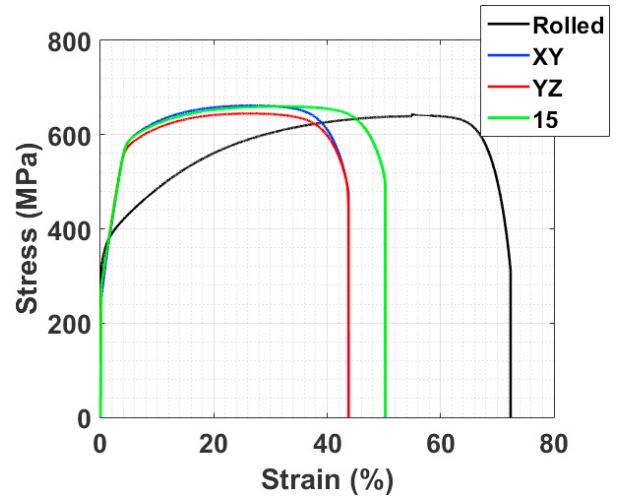


Fig. 3. Engineering stress-strain curves from uniaxial tensile testing of specimens.

top and side surfaces were arbitrarily chosen. For the rolled sample, the two sides differ in hardness by 3 HRBW (87.58 vs 84.52 HRBW). The hardness for the as-built samples were found to be more than the rolled samples: 90.54 HRBW and 92.76 HRBW for top and side surfaces, respectively. For the heat treated samples, the hardness values for both the top and the side surfaces were found to be similar at 89-90 HRBW. In general, the hardness for AM-built samples were found to be marginally higher than the rolled samples.

3.2.3. Microstructural Analysis

The microstructural analysis includes evaluation of the average planar grain size in the specimens. From the measurements, it was found that the rolled and the as-built samples had an ASTM grain size No. 9 (fine) and No. 6 (medium), respectively. Fig. 4 gives the micrograph at 100x for both the rolled and as-built samples. The melt pool lines are clearly visible in the additively fabricated as-built sample. According to the Hall-Petch relationship, smaller grain sizes lead to higher σ_y [18, 36]; thus, the Hall-Petch effect may be used to partly explain the observed results presented in Table 3.

3.3. Surface Roughness Evaluation and Improvement

One of the key disadvantages of AM is the poor surface roughness obtained in printed parts. To this end, we evaluated the surface roughness on both the top and the side surfaces. The surface texture of the as-built AM parts are shown in Figs. 5(a)-(b). The average areal surface roughness, S_a , of the top and the side surface was found to be 6.8 μm and 17 μm , respectively. The as-built surface roughness is an order of magnitude worse than the required surface roughness for the surgical instruments. To improve the surfaces finish, we evaluated three different finishing approaches: shot-peening, grinding (using mounted points), and vibratory tumbling.

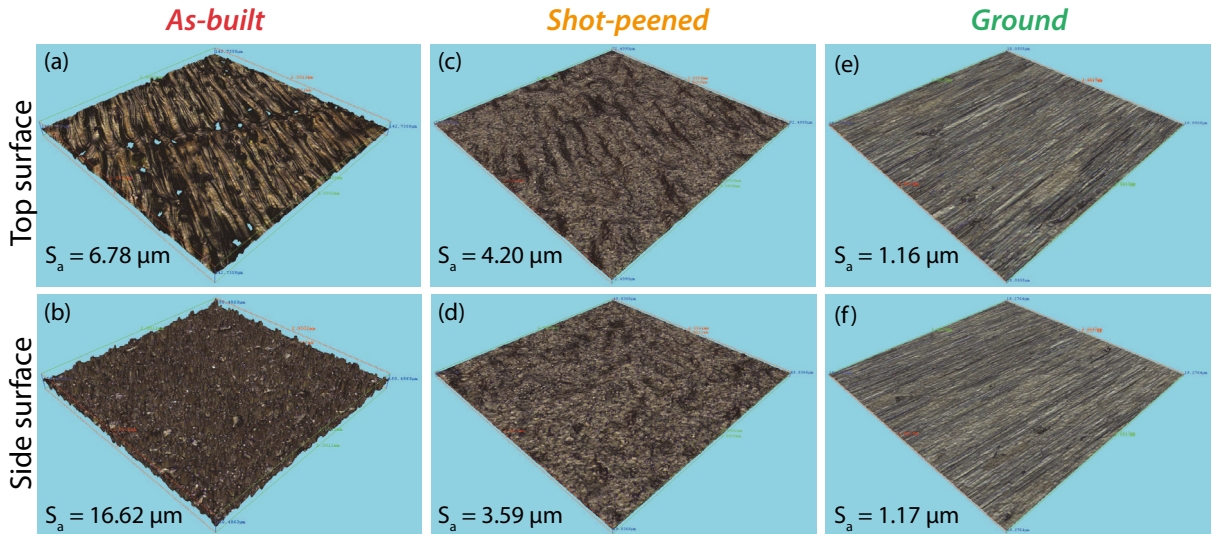


Fig. 5. Surface roughness (S_a) for top and side surfaces for (a)-(b) as-built, (c)-(d) shot-peened, and (e)-(f) ground specimens.

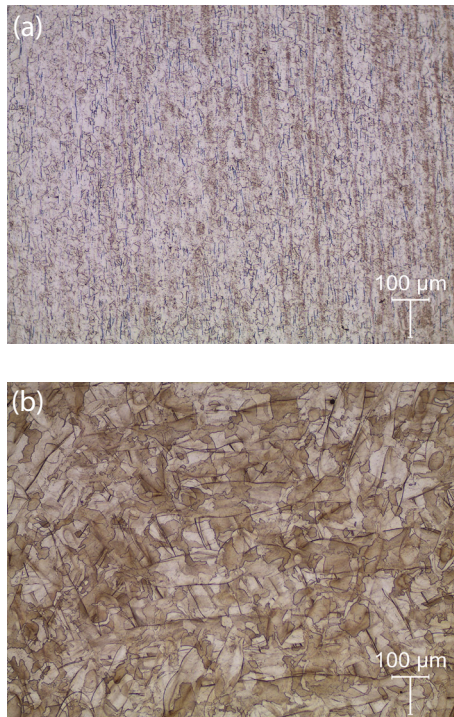


Fig. 4. (a) Rolled sample having an ASTM grain size of 9, and (b) as-built AM-sample having an ASTM grain size of 6.

Shot-peening is a commonly used method to introduce compressive stresses on the surface of a part (see, e.g., [37]). In addition, it improves the surface finish of the parts by removing the loose powder and compressing the rough surface features into the surface. A commercially available shot-peening equipment (Peenmatic 750S), which consists of a nozzle with adjustable

air pressure (0-8 bar), was used. For the as-built samples, ceramic beads were used at 5 bar pressure for 5 mins while the part is rotated manually to ensure an even coverage. The surface texture after shot peening is highlighted in the Figs 5(c)-(d). A higher reduction in surface roughness is seen for the side surfaces as they possess higher amount of loose powder. Overall, the surface roughness improved to $S_a = 4.2 \mu\text{m}$ after shot-peening.

To further improve the surface roughness of the AM-built samples, we used mounted points in cylindrical form factor (used with a rotary tool) made from abrasive materials, including silicon carbide and aluminum oxide. A relatively high rotational speed of 30,000 rev/min was used because of the smaller diameter of the mounted points. This process was able to remove the material at a higher rate and rapidly reduced the S_a down to $1.2 \mu\text{m}$, as shown in Figs. 5(e)-(f). Although, this process was able to achieve the required surface roughness, it heavily relies on generating customized tool path for a particular geometry which is difficult to achieve for complex AM-parts.

Lastly, vibratory tumbling was used to improve the surface finish for two example surgical instruments. Two different commercially-available tumbling machines, HB DECI Duo and SF MICRO Circular, were used from PostProcess Technologies. First, the parts are tumbled for 10 mins with suspended solids abrasive media (in HB DECI Duo) which reduced the surface roughness of the as-built parts from $5.84 \mu\text{m}$ to $3.30 \mu\text{m}$. Second, the parts are tumbled for 2.5 hours with H-33 ceramic media (22 deg. angle cut triangles) followed by a 30 mins. burnishing cycle (in MICRO Circular). This further reduced the roughness from $3.30 \mu\text{m}$ to $0.66 \mu\text{m}$. The results from this three-step vibratory tumbling process are discussed later in the text.

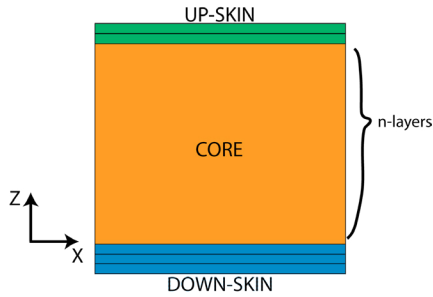


Fig. 6. The break up of parameter-set for the AM-machine [28].

3.4. Surface Roughness Optimization

In this section, printing parameters were explored to alter the surface finish on the top surface. For a part with 10 or more layers, the machine uses three different parameter sets: down-skin, core and up-skin (as shown in Fig. 6). The surface finish of the top surface in as-built condition largely depend on the up-skin parameter set. A set consists of parameters such as hatch spacing, raster speed, power and thickness. To limit the scope for this study, these parameters are varied within $\pm 20\%$ from their default values.

Fig. 7 describes the experimental matrix used for this comparative study. For this study, 10 mm x 10 mm x 10 mm coupons are printed and an area of 2 mm x 2 mm was scanned for the roughness (S_a) measurement. A low pass filter of 400 μm was used to separate roughness from the waviness profile. For each measured 3D area, the system estimates its repeatability and stores the value; the points which passes a repeatability threshold of 0.1 μm were used for the calculation of roughness.

Fig. 7 lists the calculated S_a values in μm . The arrows indicate the relative surface roughness with respect to the default parameter set. The default parameters resulted in a roughness of 6.1 μm on the top surface. An increase in laser power and a decrease in raster speed was seen to have a positive effect on the surface finish. Both the changes result in a larger melt pool which allows additional time to the melted material to flow. This causes an even flow of material, thus, improving the surface roughness of the top surface [38]. An increase in the number of up-skin layers (increase in thickness) from 2 to 3 also resulted in a finer surface finish. Similar results are obtained when hatch spacing is decreased by 10%. Overall, an increase in power by 20% has the largest effect on the surface roughness. Fig. 8 compares the difference in topography of the top surface for default parameter set and when the power is increased by 20%.

In principle, the melt-pool size can be further increased by increasing the laser power and decreasing the raster speeds to obtain improved surface finish; however, this will move the process closer to the “spatter” condition, which is undesirable and could cause increased surface roughness [39]. Note that in this small optimization study, we only changed the “top-skin” printing parameters which constitutes the top 2-3 layers and do not change the “core” parameters which is used to print the bulk

Sample No.	Hatch spacing (mm)	Speed (mm/s)	Power (W)	Thickness (mm)	Remark	S_a (μm)
0	0.09	800	135	0.04	Default	6.1
1	0.09	800	135	0.06	Thickness increase 50%	5.3
2	0.09	800	135	0.08	Thickness increase 100%	5.4
3	0.09	800	108	0.04	Power decrease 20%	9.1
4	0.09	800	162	0.04	Power increase 20%	3.4
5	0.09	640	135	0.04	Speed decrease 20%	3.7
6	0.09	960	135	0.04	Speed increase 20%	7.6
7	0.08	800	135	0.04	Hatch spacing decrease 10%	4.7
8	0.1	800	135	0.04	Hatch spacing increase 10%	6.1

Fig. 7. The experimental matrix for optimization of surface finish and corresponding results.

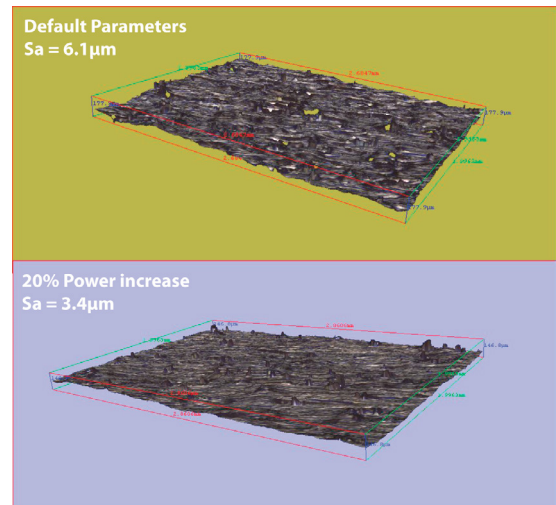


Fig. 8. Difference between the top surfaces of the as-built coupons when printed at two different power levels.

of the thickness. Therefore, this optimization routine is not expected to affect the bulk mechanical properties and rather only change the surface finish of the top surface.

4. Sample Surgical Instruments

Two custom surgical instruments—a cut guide and an acetabular shell trial—were printed to demonstrate the AM process and surface finishing approaches. These instruments were printed using the identified scaling factors to meet dimensional tolerances. Fig. 9(a) shows the printed orientation of the instruments; Fig. 9(b) shows the samples in upside-down orientation after the support removal. The outer diameter of the acetabular shell trial is measured (see Fig. 9(c)) using a caliper which reads 49.98 mm and thus satisfies the tolerance of $\pm 125 \mu\text{m}$ (nominal diameter 50 mm). Lastly, Fig. 9(d) shows the two samples after being processed in vibratory tumbling (in three-steps, see Sec. 3.3) where a sub-micron surface finish was obtained (0.6 μm - 0.9 μm S_a).

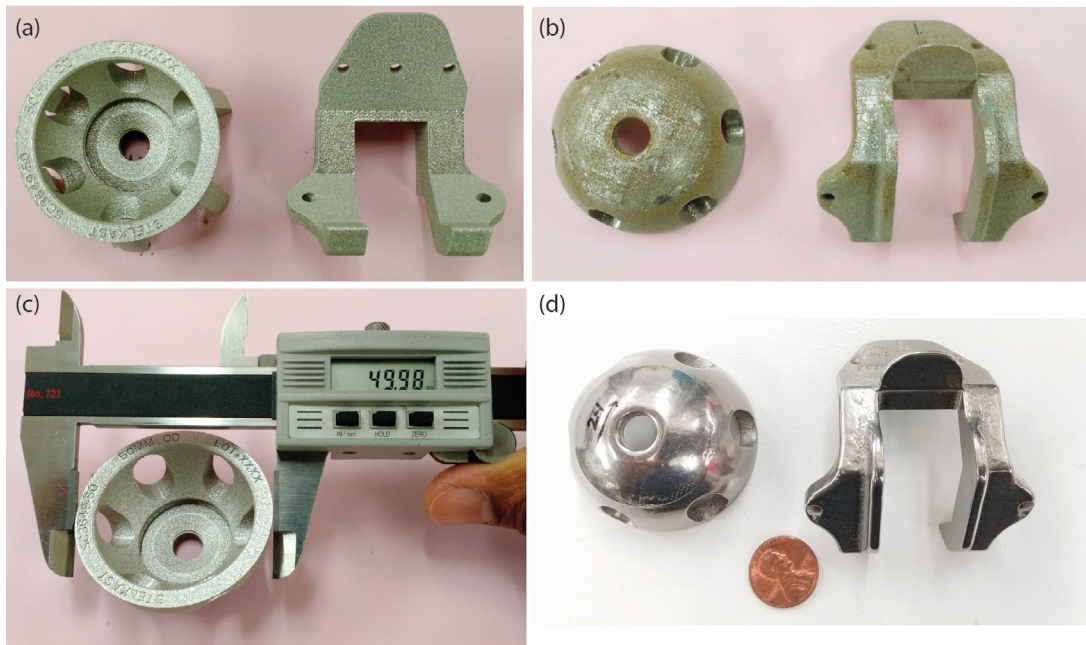


Fig. 9. Sample surgical instruments manufactured using SS 316L: (a)-(b) in as-built state with and without supports, respectively, (c) measurement of outside diameter, and (d) finished parts after vibratory tumbling.

5. Conclusions

This work presented a feasibility study towards fabricating custom-designed surgical instruments for knee and hip replacement using metal additive manufacturing. To establish the feasibility, a number of tests were conducted where the AM-built material was compared with the traditionally-manufactured (rolled) material.

The geometric characterization of the QSA helped in identifying the dimensional errors in the AM-built parts. The iterative process using a simple calibration part helped in identifying the appropriate scaling factors to achieve the desired geometric tolerance.

The mechanical testing results indicated that the traditionally fabricated and AM-fabricated parts are comparable for most of the properties (such as tensile strength, Young's modulus and hardness). The exception was ductility, which was 20-30% lower for the AM-built samples than the machined samples. The stress relieved samples show higher yield strength than the as-built samples, which was comparable to the rolled samples. Upon assessing the microstructure, fine grains (average grain size of 15 μm) was observed for rolled samples compared to medium sized grains (average grain size of 50 μm) for the as-built AM samples, which may explain the difference in the yield strength.

To improve the surface finish of the AM-built parts, both grinding (via mounted points) and vibratory tumbling was found to be successful in meeting the targeted requirements. However, vibratory tumbling was found to be better suited for complex 3D geometries such as the sample surgical instruments

discussed in the study. A study was conducted to optimize up-skin parameter set to improve the surface finish on the top surface of the as-built part. It was found that by increasing the laser power by 20%, a 45% decrease in the as-built surface roughness is observed. A decrease in surface roughness is also achieved by decreasing the laser scan speed and an increase in the number of up-skin layers. Lastly, two sample surgical instruments were successfully fabricated and post processed, meeting all the aforementioned requirements for surgical instruments.

Acknowledgments

This project was funded by America Makes (FA8650-12-2-7230) and Research for Advanced Manufacturing in Pennsylvania (RAMP). We acknowledge the support of our industrial partner, StelKast Inc., for providing CAD models of sample surgical instruments and supplying the traditionally manufactured 316L stainless steel samples for testing.

References

- [1] Sunpreet Singh and Seeram Ramakrishna. Biomedical applications of additive manufacturing: Present and future. *Current Opinion in Biomedical Engineering*, 2:105–115, 2017.
- [2] Martin J Polinski and Paula M Berg. Integrated Production of Patient-Specific Implants and Instrumentation, aug 2010.
- [3] Wilfried Vancraen and Michel Janssens. Additive manufacturing flow for the production of patient-specific devices comprising unique patient-specific identifiers, may 2012.

- [4] James Schroeder, Steven Goodman, and Kyu-Jung Kim. Personal fit medical implants and orthopedic surgical instruments and methods for making, may 2007.
- [5] Richard Bibb, Dominic Eggbeer, Peter Evans, Alan Bocca, and Adrian Sugar. Rapid manufacture of custom-fitting surgical guides. *Rapid Prototyping Journal*, 2009.
- [6] Risto Kontio. Designing and Additive Manufacturing A Prototype for A Novel Instrument for Mandible Fracture Reduction. *Surgery: Current Research*, 03(01), 2013.
- [7] Shayne Kondor, CAPT Gerald Grant, Peter Liacouras, M A J James R Schmid, L T C Michael Parsons, Vipin K Rastogi, Lisa S Smith, Bill Macy, Brian Sabart, and Christian Macedonia. On demand additive manufacturing of a basic surgical kit. *Journal of Medical Devices*, 7(3):30916, 2013.
- [8] Timothy J. Horn and Ola L A Harrysson. Overview of current additive manufacturing technologies and selected applications. *Science Progress*, 95(3):255–282, 2012.
- [9] Brett Lyons. Additive Manufacturing in Aerospace: Examples and Research Outlook. *The Bridge*, 2012.
- [10] Adrián Uriondo, Manuel Esperon-Miguez, and Suresh Perinpanayagam. The present and future of additive manufacturing in the aerospace sector: A review of important aspects, 2015.
- [11] Mohd. Javaid and Abid Haleem. Additive manufacturing applications in medical cases: A literature based review. *Alexandria Journal of Medicine*, 2017.
- [12] C. Lee Ventola. Medical Applications for 3D Printing: Current and Projected Uses. *Information and Software Technology*, 2009.
- [13] Miika Salmi, Jukka Tuomi, KaijaStiina Paloheimo, Roy Björkstrand, Markku Paloheimo, Jari Salo, Risto Kontio, Karri Mesimäki, and Antti A. Mäkitie. Patient specific reconstruction with 3D modeling and DMLS additive manufacturing. *Rapid Prototyping Journal*, 18(3):209–214, 2012.
- [14] Ben Vandenbroucke and JeanPierre Kruth. Selective laser melting of bio-compatible metals for rapid manufacturing of medical parts. *Rapid Prototyping Journal*, 13(4):196–203, 2007.
- [15] Xiaojian Wang, Shanqing Xu, Shiwei Zhou, Wei Xu, Martin Leary, Peter Choong, M. Qian, Milan Brandt, and Yi Min Xie. Topological design and additive manufacturing of porous metals for bone scaffolds and orthopaedic implants: A review, 2016.
- [16] Swee Leong Sing, Jia An, Wai Yee Yeong, and Florencia Edith Wiria. Laser and electron-beam powder-bed additive manufacturing of metallic implants: A review on processes, materials and designs, 2016.
- [17] Chandrika Kamath, Bassem El-Dasher, Gilbert F. Gallegos, Wayne E. King, and Aaron Sisto. Density of additively-manufactured, 316L SS parts using laser powder-bed fusion at powers up to 400 W. *International Journal of Advanced Manufacturing Technology*, 74(1-4):65–78, 2014.
- [18] J. A. Cherry, H. M. Davies, S. Mehmood, N. P. Lavery, S. G R Brown, and J. Sienz. Investigation into the effect of process parameters on microstructural and physical properties of 316L stainless steel parts by selective laser melting. *The International Journal of Advanced Manufacturing Technology*, 76(5-8):869–879, 2015.
- [19] Jordi Delgado, Joaquim Ciurana, and Ciro A. Rodríguez. Influence of process parameters on part quality and mechanical properties for DMLS and SLM with iron-based materials. In *International Journal of Advanced Manufacturing Technology*, volume 60, pages 601–610, 2012.
- [20] M. Simonelli, Y. Y. Tse, and C. Tuck. Effect of the build orientation on the mechanical properties and fracture modes of SLM Ti-6Al-4V. *Materials Science and Engineering A*, 616:1–11, 2014.
- [21] Marcin B Bauza, Shawn P Moylan, Robert M Panas, Stephen C Burke, E Martz, John S Taylor, Richard H Knebel, Raghuram Bhogaraju, and Maple Grove. Study of accuracy of parts produced using additive manufacturing. In *2014 ASPE Spring Topical Meeting: Dimensional Accuracy and Surface Finish in Additive Manufacturing*, pages 1–8, 2014.
- [22] G. Ziólkowski, E. Chlebus, P. Szymczyk, and J. Kurzac. Application of X-ray CT method for discontinuity and porosity detection in 316L stainless steel parts produced with SLM technology. *Archives of Civil and Mechanical Engineering*, 14(4):608–614, 2014.
- [23] S. Dadbakhsh, L. Hao, and N. Sewell. Effect of selective laser melting layout on the quality of stainless steel parts. *Rapid Prototyping Journal*, 18(3):241–249, 2012.
- [24] Giovanni Strano, Liang Hao, Richard M. Everson, and Kenneth E. Evans. Surface roughness analysis, modelling and prediction in selective laser melting. *Journal of Materials Processing Technology*, 213(4):589–597, 2013.
- [25] K. Alrbaey, D. Wimpenny, R. Tosi, W. Manning, and A. Moroz. On optimization of surface roughness of selective laser melted stainless steel parts: A statistical study. *Journal of Materials Engineering and Performance*, 23(6):2139–2148, 2014.
- [26] Warren G Ragland III. Surface Finish Analysis of Surgical Tools Created by Direct Metal Laser Sintering and Subtractive Manufacturing. *2012 NCUR*, 2012.
- [27] ASTM International. ASTM F899-12b, Standard Specification for Wrought Stainless Steels for Surgical Instruments. 2012.
- [28] EOS. <http://www.eos.info/eos-m290>, 2015.
- [29] K. Saeidi, X. Gao, F. Lofaj, L. Kvetková, and Z. J. Shen. Transformation of austenite to duplex austenite-ferrite assembly in annealed stainless steel 316L consolidated by laser melting. *Journal of Alloys and Compounds*, 633:463–469, 2015.
- [30] Bohan Hao, Emrullah Korkmaz, Bekir Bediz, and O Burak Ozdoganlar. A novel test artifact for performance evaluation of additive manufacturing processes. In *American Society for Precision Engineering Conference*. *Google Scholar*, 2014.
- [31] ASTM. E8/E8M standard test methods for tension testing of metallic materials. *Annual Book of ASTM Standards 4*, i:1–27, 2010.
- [32] Erva Ulu, Emrullah Korkmaz, Kubilay Yay, O. Burak Ozdoganlar, and Levant Burak Kara. Enhancing the Structural Performance of Additively Manufactured Objects Through Build Orientation Optimization. *Journal of Mechanical Design*, 2015.
- [33] ASTM. ASTM E112-12 : Standard Test Methods for Determining Average Grain Size. *ASTM International*, E112-12:1–27, 2012.
- [34] ASTM. Standard Test Methods for Rockwell Hardness of Metallic Materials. *ASTM International*, pages 1–38, 2015.
- [35] John J. Lewandowski and Mohsen Seifi. Metal Additive Manufacturing: A Review of Mechanical Properties. *Annual Review of Materials Research*, 2016.
- [36] Niels Hansen. Hall-petch relation and boundary strengthening. *Scripta Materialia*, 2004.
- [37] Shengping Wang, Yongjun Li, Mei Yao, and Renzhi Wang. Compressive residual stress introduced by shot peening. *Journal of Materials Processing Technology*, 1998.
- [38] F. Calignano, D. Manfredi, E. P. Ambrosio, L. Iuliano, and P. Fino. Influence of process parameters on surface roughness of aluminum parts produced by DMLS. *International Journal of Advanced Manufacturing Technology*, 2013.
- [39] Luke Scime and Jack Beuth. Using machine learning to identify in-situ melt pool signatures indicative of flaw formation in a laser powder bed fusion additive manufacturing process. *Additive Manufacturing*, 2019.